energy&fuels

pubs.acs.org/EF
Article

Dissociation Line and Driving Force for Nucleation of the Multiple Occupied Hydrogen Hydrate from Computer Simulation

Published as part of Energy & Fuels special issue "2025 Pioneers in Energy Research: E. Dendy Sloan".

Miguel J. Torrejón, Samuel Blazquez, Jesús Algaba, Maria M. Conde,* and Felipe J. Blas*

Cite This: *Energy Fuels* 2025, 39, 15184−15197

Read Online

ACCESS | Metrics & More | Article Recommendations

ABSTRACT: In this work, we determine the dissociation temperature of hydrogen (H_2) hydrate by computer simulation using two different methods. In both cases, the molecules of water and H_2 are modeled using the TIP4P/Ice and a modified version of the Silvera and Goldman models, respectively, and the Berthelot combining rule for the cross water−H_2 interactions has been modified. The first method used in this work is the solubility method, which consists of determining the solubility of H_2 in an aqueous phase when in contact with the H_2 hydrate ($H-L_w$) phase and when in contact with the pure H_2 phase ($L_w-L_{H_2}$) at different temperatures. At a given pressure value, both solubility curves intersect at the temperature (T_3) at which the three phases coexist in equilibrium. Following this approach, we determine the dissociation temperature of H_2 hydrate at 185 MPa finding a good agreement with the data previously reported in the literature. We also analyze the effect of the multiple occupancy of the D, or small, and H, or large, cages of the sII hydrate structure. We conclude that the T_3 value is barely affected by the occupancy of the H_2 hydrate at 185 MPa. From the analysis of the solubility curves and performing extra bulk simulations of the three phases involved in the equilibrium, we also determine the driving force for nucleation ($\Delta\mu_N^{EC}$) at 185 MPa as a function of the supercooling degree and the H_2 hydrate occupancy. We determine that, thermodynamically, the most favored occupancy of the H_2 hydrate consists of 1 H_2 molecule in the D cages and 3 in the H cages (i.e., 1−3 occupancy). We also conclude that the double occupancy of the small D cages is not favored because the $\Delta\mu_N^{EC}$ values obtained for this occupancy are the most positive ones. The second approach used in this work is the direct coexistence technique using an initial H_2 hydrate phase with 1−3 occupancy. We also propose a new modification of the Berthelot combining rule to improve the predictions of the T_3 values. Following this method, we determine the T_3 at 100, 185, and 300 MPa finding excellent agreement with the experimental data.

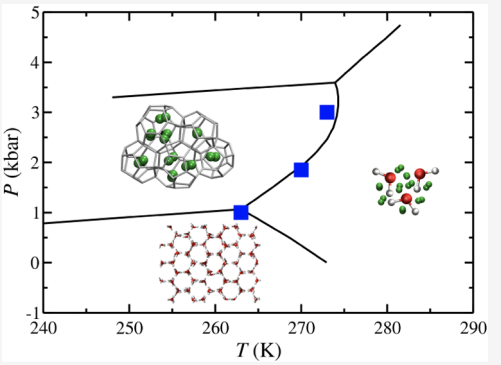

INTRODUCTION

Clathrates are nonstoichiometric inclusion crystalline compounds consisting of a network of hydrogen-bonded molecules (host) forming cages in which small molecules (guest) such as hydrogen (H_2), nitrogen (N_2), carbon dioxide (CO_2), and methane (CH_4), among many others, can be encapsulated under the appropriate thermodynamic conditions.[1,2] When water acts as the host molecule, these structures are specifically termed clathrate hydrates or simply hydrates. Among the many hydrates applications such as CO_2 capture[3−10] or N_2 recovery from industrial emissions,[11,12] it is interesting to remark on their energetic applications. In nature, vast deposits of natural gas exist as hydrates. According to the last estimations, conventional natural gas deposits correspond to 20% of the total natural gas present in nature, while the remaining 80% is trapped as hydrate on the seabeds and permafrost areas.[13−15] Thus, methane hydrate represents an interesting alternative as a source of energy.

Although the use of hydrates as a source of natural gas would help to alleviate the global energy crisis that the world is facing today, it is also necessary to mitigate anthropogenic carbon emissions in order to palliate climate change. However, reducing carbon emissions while ensuring the energy needs of a growing population are met is not an easy task. In this regard, the use of hydrates of H_2, in combination with hydrate promoters, as strategic materials for gas transport and storage, is one of the most significant and promising applications of hydrates in the environmental, energetic, and economic context. This represents a potential alternative to metal

Received: February 25, 2025
Revised: June 20, 2025
Accepted: June 24, 2025
Published: July 1, 2025

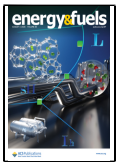

https://doi.org/10.1021/acs.energyfuels.5c01012
Energy Fuels 2025, 39, 15184−15197

hydrides that are currently in use. However, the use of metal hydrides as H_2 storage media has not yet been implemented due to a lack of information regarding the thermodynamic and kinetic properties of these compounds.[11,16−18] The utilization of H_2 hydrates in this context would result in a reduction in raw material costs while maintaining a comparable volumetric storage capacity. In order to achieve this, it is necessary a deep understanding of the phase equilibria and the kinetics of the formation and growth of these hydrates, with special emphasis on which are the factors that rule the occupancy of these hydrates.[17−34]

At high pressures and low temperatures, H_2 hydrates crystallize in the so-called sII structure with 136 water molecules distributed in 16 D (pentagonal dodecahedron or 5^{12}) cages and 8 H (hexakaidecahedron or $5^{12}6^4$) cages. The D, or small, cages are better stabilized by small molecules such as H_2 or N_2 while the H, or large, cages are better stabilized by larger molecules such as propane. However, it is interesting to remark that the large H cages can be also stabilized by the multiple occupancy of small molecules such as H_2 or N_2.[1,2] From an experimental point of view, the analysis of hydrate occupancy is a challenging endeavor, primarily due to the extreme conditions required for their formation and equilibrium stability. These conditions include high pressure and low temperature, which present significant difficulties in producing homogeneous samples for analysis. Furthermore, the experimental measurement of equilibrium properties, such as the lattice constants and cage occupancies, is not a straightforward process.[19,21−24,35] In a series of recent works, Zhang et al.[36−38] provide a detailed analysis of the H_2 hydrate formation in the presence of several hydrate promoters (tetrahydrofuran, L-val, and 1,3-dioxolane). They studied the formation kinetics of the H_2 hydrate under the presence of different thermodynamic and kinetic promoters as well as a detailed analysis of how the hydrate promoter concentration affects the H_2 hydrate formation. They study the occupancy of both types of sII hydrate cages by using Raman spectroscopy, which is a special interesting topic due to the possibility of using hydrates to store H_2, concluding that H_2 molecules solely occupy the small D cages of the sII hydrates with thermodynamic hydrate promoters occupying the large H cages. At this point, it is interesting to remark that although tetrahydrofuran is a very special thermodynamic hydrate promoter since it is able to form a hydrate by itself,[13,39−49] the 1,3-dioxolane is less toxic[50] and, hence, more friendly from an environmental point of view, which is a prerequisite for large-scale application of hydrate-based H_2 storage technology.[38]

In order to use hydrates as H_2 storage media, it is necessary to obtain a deep understanding of how the thermodynamic conditions affect the occupancy of these compounds since an increment of the occupancy implies an improvement of the storage capacity. In this respect, theoretical and simulation approaches provide an interesting molecular perspective to study the occupancy of these hydrates. Although the occupancy of H_2 hydrates has been the subject of several studies, there is still an open debate about the amount of H_2 that can be encapsulated inside the small, D, and large, H cages of the sII hydrate structure. From an experimental point of view, Mao et al.[19,24] state that the double occupancy of both types of cage is possible. This has been corroborated by Belosudov et al.[20] from theoretical calculations and by Liu et al.[27] from ab initio computations. However, from simulations, there is still controversy over the H_2 hydrate occupancy. Alavi et al.[29] state that, at low pressures (below 2.5 kbar), the most stable occupancy of the sII H_2 hydrate consists of 4 H_2 molecules in the H cages while the D cages remain single occupied. They also remark that the double occupancy of the D cages provokes an increase in the structure energy and tetragonal distortions of the hydrate unit cell. The same conclusion was found by Papadimitriou et al.[30] at pressures between 380 and 450 MPa. They also affirm that the most stable occupancy consists of 4 and 1 H_2 molecules in the H and D cages, respectively. They also study the effect of lattice constant on the storage capacity of hydrogen hydrates[26] and the impact of different force fields on the H_2 hydrate storage predictions.[33] Also in the works of Katsumasa et al.[25] and Chun and Lee[32] it is shown that H cages can be multiply occupied while D cages remain single occupied in most cases. Contrary to the previous simulation studies, Brumby et al.[17] performed a detailed analysis of the H_2 hydrate occupancy from Gibbs ensemble Monte Carlo simulations. They concluded that the occupancy of D cages is not limited to only single occupancy at pressures below 400 MPa, although only a small percentage of them in the hydrate structure were doubly occupied.

In this work, we study the dissociation temperature of the sII H_2 hydrate at 185 MPa as a function of the multiple occupancy of both the D and H cages. At the dissociation temperature (T_3), the system under study presents a three-phase equilibrium. The three phases involved are a H_2 hydrate phase, an aqueous phase with the corresponding equilibrium H_2 solubility, and a pure H_2 phase. The dissociation temperature at 185 MPa and for various H_2 hydrate occupancies are obtained using molecular dynamics simulations and the solubility method.[51−55] We use the TIP4P/Ice[56] and a modified version of the Silvera and Goldman[29,57] models to describe the molecules of water and H_2 respectively. We analyze the effect of the occupancy of the large H cages from single to quadruple occupancy and the occupancy of the small D cages from single to double occupancy on the dissociation temperature. We also obtained the driving force for nucleation, $\Delta\mu_N$, at 185 MPa as a function of the H_2 hydrate occupancy and the supercooling degree. Taking into account the dissociation temperature and the driving force for nucleation results obtained for the different occupancies, we study the dissociation temperature of the most favored one (3 and 1 H_2 molecules in the H and D cages, respectively) from 100 to 300 MPa. Finally, we propose a new modification of the Berthelot combining rule to improve the simulation results and predict accurately the experimental data.[21,35] It is important to remark that, experimentally, hydrate phase diagrams are studied by performing experiments at different thermodynamic conditions and monitoring when a phase transition takes place.[21,35] Notice that this implies the crystallization of the H_2 hydrate from an H_2 aqueous solution. Homogeneous nucleation at the thermodynamic equilibrium conditions is a rare event that can only be studied from simulation using special and computationally expensive techniques, which hinders employing the same specific conditions and procedures as experiments. However, the same information can be obtained by simpler and cheaper simulation methodologies such as the direct coexistence technique[11,18,48,58−66] and the solubility method.[51−55] Notice that, for a given pressure, there is only a possible T_3 value that should be independent of the

https://doi.org/10.1021/acs.energyfuels.5c01012
Energy Fuels 2025, 39, 15184−15197

Table 1. Nonbonded Interaction Parameters and Geometry Details of TIP4P/Ice Water[56] and Modified SG H_2[18,29,68] Molecular Models Employed in This Work

atom	σ (Å)	ε/k_B (K)	q (e)	geometry details	
			Water (TIP4P/Ice)		
O	3.1668	106.1	-	d_{OH} (Å)	0.9572
H	-	-	0.5897	H−O−H (deg)	104.5
M	-	-	−1.1794	d_{OM} (Å)	0.1577
			H_2 (SG)		
H	0	0	0.4932	d_{HH} (Å)	0.7414
mass center	3.038	34.302	−0.9864		

specific conditions at which experiments and simulations are performed.

The organization of this article is as follows: In the Models, Simulations Details, and Methodology section, we describe the models, simulation details, and methodology used in this work. The results obtained, as well as their discussion, are described in the Results section. Finally, the conclusions are presented in the Conclusions section.

MODELS, SIMULATION DETAILS, AND METHODOLOGY

In this work, all molecular dynamics simulations have been carried out using the GROMACS[67] (2016.5 double−precision version) software package. Water molecules are modeled using the widely known TIP4P/Ice model.[56] Following the work of Alavi et al.,[29] we employ a modified version of the Silvera and Goldman[57] (SG) H_2 model based on the well depth and potential minimum of the original SG isotropic isolated pair potential for gas-phase hydrogen. This modified version simplifies the original SG interaction potential and makes it more suitable for high-performance simulations.[18] In this model, the H_2 molecule is described by two hydrogen atoms linked by a rigid bond of 0.7414 Å with a Lennard−Jones (LJ) interactive site in the molecule's center of mass. Also, positive charges are placed on the hydrogen centers while the negative charge is placed in the molecule's center of mass together with the LJ interactive site. A summary of the molecular model details of both compounds is shown in Table 1.

In all cases the nonbonded cross interactions between unlike groups are calculated using the Lorentz−Berthelot combining rule. However, as in the original work of Michalis et al.,[18] we modify the Berthelot combination rule between the oxygen group from the water molecule and the LJ interactive site from the H_2 molecule. This modification improves the predictions of the H_2 solubility in water and the three-phase coexistence temperature (T_3) determination in the 273.15−323.15 K and 100−300 MPa range of temperatures and pressures, respectively. In particular, the Berthelot combination rule is modified by a χ factor whose value is a function of the temperature

$$\epsilon_{O-MH_2} = \chi(\epsilon_{OO}\epsilon_{MH_2-MH_2})^{1/2} \quad (1)$$

$$\chi = a_1 \exp\left(-\frac{T}{a_2}\right) + a_0 + b_0 \quad (2)$$

where χ is the Berthelot modifier factor, ϵ_{OO} and $\epsilon_{MH_2-MH_2}$ are the LJ well-depth associated with the oxygen atom from the water molecule and the center of mass of the H_2 molecule, respectively. The a_0, a_1, and a_2 parameters are taken from the work of Michalis et al.,[18] and the b_0 parameter value is proposed in this work. Particularly, the model proposed by these authors corresponds to values a_0 = 0.649194, a_1 = 0.12085, and a_2 = −186.29458 K. Notice that when b_0 = 0, eq 2 is identical to that proposed by Michalis et al.[18]

Although the original expression for the χ factor proposed by Michalis et al.[18] provides an excellent agreement between the experimental and the simulated solubility of H_2 in water, and also improves the prediction of the three-phase coexistence temperature (T_3) in the 100−300 MPa range of pressure, the T_3 values obtained from simulation still underestimate the experimental T_3 value (see Direct Coexistence Method section for further details). Hence, in this work, we propose a new χ expression based on the original one proposed by Michalis et al.[18] We introduce the b_0 parameter in eq 2 in order to improve the T_3 value obtained from molecular dynamic simulations. In this work, b_0 has a value of 0.1. The addition of this factor provides an excellent prediction of the H_2 hydrate T_3 value but slightly overestimates the H_2 solubility in water. This b_0 value was obtained by determining the predicted T_3 value by using different χ values. In all cases, we used the initial value obtained from the original χ expression, and T_3 was evaluated at 100, 185, and 300 MPa by systematically varying χ in increments of 0.1. We determine that just a 0.1 increment is enough to provide an accurate description of the T_3 value since an additional increment of the χ factor (b_0 = 0.2) overestimates it. A detailed analysis of the solubility of H_2 in water using the TIP4P/Ice and SG models for the water and H_2 molecules as a function of the χ factor can be found in the original work of Michalis et al.[18]

In this work, the Verlet leapfrog[69] algorithm with a time step of 2 fs is used to solve the motion equations of Newton. Also, we use the Nosé−Hoover thermostat,[70] with a time constant of 2 ps, and the Parrinello−Rahman barostat,[71] with a time constant of 2 ps and a 5×10^{-5} compressibility value, to ensure that simulations are performed at constant temperate and pressure. Following the original work of Michalis et al.,[18] we use a cutoff value of 1.1 nm for the Coulombic and dispersive interactions. We do not use long-range corrections for the dispersive LJ interactions but Particle-Mesh Ewald (PME)[72] corrections are used for the Coulombic potential.

In order to determine the three-phase coexistence temperature, we employed two different methods. First, we employ the solubility method[51−55] and the original modification of the χ factor proposed by Michalis et al.[18] (i.e., b_0 = 0). Following the procedure used in our previous works,[52−55] the T_3 value is determined by studying the solubility of H_2 in an aqueous solution phase when it is in contact via a planar interface with an initial pure H_2 phase (L_w−L_{H_2} two-phase equilibria) and when in contact with a hydrate phase (H−L_w two-phase equilibria). The number of molecules used in each case is specified in the corresponding sections. According to the

https://doi.org/10.1021/acs.energyfuels.5c01012
Energy Fuels 2025, 39, 15184−15197

solubility method, the T_3 value is determined by representing the solubility values obtained from both equilibria at a constant pressure and as a function of the temperature. The solubility of H_2 in the aqueous phase, when it is in contact with the H_2-rich liquid phase, decreases with temperature, as it happens with the solubility of most gases in water; in contrast, the solubility of H_2, when it is in contact with the hydrate phase, increases with temperature. Note that this behavior with temperature is similar to that observed when a solid is dissolved in water. In the intersection of both curves, the aqueous phase has reached the same thermodynamic equilibrium state (monitoring by the H_2 solubility value) when in contact with a H_2 hydrate phase and when in contact with a pure liquid H_2 phase separately, i.e., the temperature at which both curves cross is the temperature at which the liquid water, hydrate, and H_2 liquid phases are in equilibrium, which represents the so-called T_3 at the corresponding pressure. In this work, the T_3 value is determined using the solubility method and the χ factor proposed by Michalis et al.[18] at P = 185 MPa. We also analyze the effect of the H_2 hydrate occupancy on the T_3 value. The sII unit cell hydrate structure is built up by 16 D (small) and 8 H (large) hydrate cages. In this work, we calculated the T_3 at 185 MPa when the D, or small, cages are singly occupied and the H, or large, cages are occupied by 1, 2, 3, and 4 H_2 molecules (called from now on 1−1, 1−2, 1−3, and 1−4 occupancies). Also, we analyze the effect of double occupancy in the small D cages when 2 and 4 H_2 molecules occupy the small D and large H cages respectively (2−2 and 2−4 occupancies). Unfortunately, although we generate and equilibrate a bulk 2−4 H_2 hydrate phase, it becomes unstable when it is put in contact with an aqueous phase. Therefore, we conclude that the 2−4 occupancy is not stable and can not be simulated under the thermodynamic conditions considered in this work.

The L_w−L_{H_2} equilibria simulations are performed in the NP_zT ensemble, i.e., only the P_z component of the pressure tensor, which is perpendicular to the L_w−L_{H_2} planar interface, is fixed by the barostat. The H−L_w equilibria simulations are carried out in the anisotropic NPT ensemble i.e., each side of the simulation box is allowed to fluctuate independently to keep the pressure constant and to avoid any stress from the solid hydrate structure. Also, we perform extra bulk simulations, in the isotropic NPT ensemble, of pure water, pure H_2, and pure H_2 hydrate phases with different occupancy levels to determine the driving force for nucleation as a function of the H_2 hydrate occupancy and the supercooling degree. The water and H_2 pure bulk phases are built up by 1000 molecules of water and H_2, respectively, and the bulk H_2 hydrate phase is obtained by replicating the unit cell twice in each space direction taking into account the corresponding H_2 occupancy.

The second method used in this work is the direct coexistence technique.[11,18,48,58−65,73−80] Following this method, the three phases involved in the equilibrium (H−L_w−L_{H_2}) are placed together in the same simulation box. By fixing the pressure and varying the temperature, one can analyze the behavior of the three-phase system and determine the T_3 value. If the fixed temperature is below the T_3, at a given pressure value, the aqueous L_w phase becomes unstable and the hydrate phase grows until extinguishing the L_w or the L_{H_2} phase depending on the number of molecules of water and guest in both phases. Contrarily, if the fixed temperature is above the T_3 value, the hydrate phase becomes unstable and it melts, obtaining a L_w−L_{H_2} equilibria. In this work, the T_3 value is obtained at three different pressures (100, 185, and 300 MPa), using an initial hydrate phase seed with a 1−3 occupancy and using the modified χ factor expression proposed in this work (eq 2 with b_0 = 0.1). As in the study of the H−L_w equilibria, simulations are performed in the anisotropic NPT ensemble to avoid any stress from the solid hydrate structure.

RESULTS

In this section, we present a detailed analysis of the H_2 hydrate dissociation temperature. First, we focus on determining the T_3 value at 185 MPa as a function of the H_2 hydrate occupancy using the solubility method and a modification of the Berthelot combining rule already presented in the literature by Michalis et al.[18] We also study the driving force for nucleation of the H_2 hydrate as a function of the supercooling degree for the five different occupancies studied in this work at 185 MPa. Finally, we propose a modification of the χ factor expression proposed by Michalis et al.[18] and we determine the T_3 at 100, 185, and 300 MPa using the direct coexistence technique. The new expression for the χ factor proposed in this work provides the same T_3 values from simulations as those reported from experiments in the literature between the error bars. At this point, it is important to remark that the χ original factor expression was proposed to match the simulated and experimental solubility of H_2 in an aqueous phase. This resulted in an improvement of the T_3 prediction using the classical Lorentz−Berthelot combining rule, but the T_3 values obtained with this modification of the Berthelot combining rule still slightly underestimate the experimental T_3 value. On the other hand, the new expression for the χ factor proposed in this work provides an excellent prediction of the T_3 values but slightly overestimates the H_2 solubility in water.

Solubility Method. In order to determine the T_3 value at 185 MPa through the solubility method, first it is necessary to obtain the solubility of H_2 in water when an aqueous phase (L_w) is in contact with a pure H_2 phase (L_{H_2}) and when in contact with a H_2 hydrate phase (H). First, we focus on the L_w−L_{H_2} equilibria and then in the H−L_w equilibria.

L_w−L_{H_2} Equilibria: Solubility of H_2 in Liquid Water and Interfacial Tension. We study the L_w−L_{H_2} equilibria behavior by running NP_zT simulations at 185 MPa and 230, 240, 250, 260, 270, and 280 K. The initial simulation box is built up by a pure water phase with 2800 water molecules and a pure H_2 phase with 1400 H_2 molecules. Both phases are put in contact via a planar interface along the z-direction. The xy interfacial area remains constant throughout the whole simulation since the values of $L = L_x = L_y$ are fixed at 3.8 nm. Finally, the average L_z side of the simulation box is ≈9.8 nm and both phases approximately fill half of the simulation box along the z-axis direction. Due to the low solubility of H_2 in water, simulations are run for 800 ns. The first 400 ns are taken as the equilibration period, and the last 400 ns are taken as the production period.

The H_2 solubility values in the aqueous phase are calculated from the analysis of the density profiles. These are obtained by dividing the simulation box into 200 slabs and assigning the center of mass of each molecule to the corresponding slab. Finally, the mass density profile is obtained by multiplying the molar density profile of each compound by its corresponding molar mass. The solubility of H_2 in the aqueous phase at each

https://doi.org/10.1021/acs.energyfuels.5c01012
Energy Fuels 2025, 39, 15184−15197

temperature is obtained by averaging for each component the values of the density profiles by using each slab belonging to the aqueous phase. The error bars of the densities of water and H_2 in the aqueous phase at each temperature are obtained as the average standard deviation. The H_2 solubility error bars are obtained by propagating the density errors obtained for both components. Calculations are performed far enough from the interface to avoid the effect of the interface on the average H_2 solubility determination. Figure 1 shows the H_2 solubility

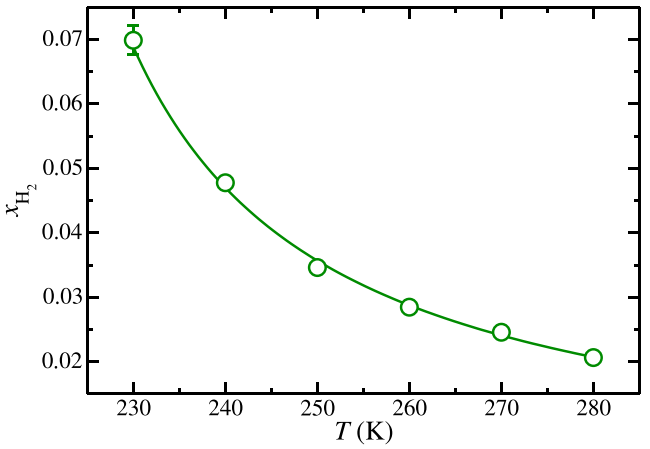

Figure 1. H_2 solubility in the aqueous solution phase as a function of temperature at 185 MPa. The green open-circle symbols represent the solubility values obtained from the L_w–L_{H_2} NP_zT molecular dynamic simulations performed in this work. The green curve is included as a guide for the eye.

values in the aqueous phase obtained in this work at 185 MPa and several temperatures. The results obtained in this work are in good agreement with those reported by Michalis et al.[18] As can be seen in Figure 1, the solubility of H_2 in the aqueous phase decreases when the temperature is increased. This is the expected behavior of the solubility of a gas in water with the temperature. Notice that, when the temperature is increased, the H_2 solubility varies more steeply at the lowest temperature values studied in this work.

From the analysis of the L_w–L_{H_2} it is possible to determine the interfacial tension between the aqueous and the H_2 phases from the diagonal components of the pressure tensor.[81−83] As in the case of the density profiles, the interfacial tension at each temperature is determined from the last 400 ns of the L_w–L_{H_2} molecular dynamic simulations. In order to obtain an estimation of the errors, the 400 ns of the production period are divided into 10 blocks of 40 ns. The final value of the interfacial tension is obtained by averaging the value of each block. Finally, uncertainties are estimated as the standard deviation of the average.[84] As can be observed in Figure 2, the L_w–L_{H_2} interfacial tension decreases steeply when the temperature is increased from 230 to 260 K until reaches an almost plateau value at 270 and 280 K. Similar behavior was found in a previous work[54] when the liquid water–liquid nitrogen (L_w–L_{N_2}) interfacial tension was analyzed at 1000 and 1500 bar from 245 to 300 K. Unfortunately, as far as the authors know, there are no experimental data available in the literature to compare with the results obtained in this work.

H–L_w Equilibria: Solubility of H_2 in Liquid Water When It Is in Contact with H_2 Hydrate. Following an approach similar

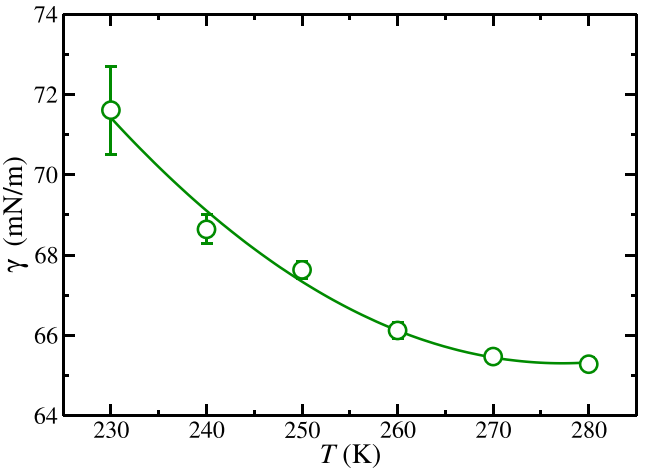

Figure 2. L_w–L_{H_2} interfacial tension, γ, as a function of the temperature at 185 MPa. The results obtained in this work from molecular dynamic NP_zT simulations, and its error bars, are represented as open green circles. The green curve is included as a guide for the eyes.

to that in the L_w–L_{H_2} equilibria, we study the solubility of H_2 in an aqueous phase when it is in contact via a planar interface with a H_2 hydrate phase (H–L_w). We obtain the H_2 solubility values at 185 MPa from 250 to 270 K by running *NPT* simulations. The barostat is applied anisotropically in the three space directions to avoid stress from the solid H_2 hydrate structure. Simulations are run for 800 ns, with the first 200 ns being considered as the equilibration period and the last 600 ns being considered as the production period. In this case, the initial simulation box is prepared as follows. The hydrate is formed from 1088 molecules of water and a different number of H_2 molecules depending on the occupation level (see Table 2). As can be seen, this corresponds to a $2 \times 2 \times 2$ unit cell of the sII hydrate structure with different occupancies and space groups of the unit cell $Fd3m$. The proton disorder is obtained using the algorithm of Buch et al.[85] Once the hydrate phase is equilibrated, it is put in contact with a water-liquid phase.

Due to the low solubility of H_2 in water, the initial aqueous phase in contact with the H_2 hydrate phase is built up as an initial pure water phase. Both phases are in contact via a planar interface along the z–direction. In order to reach the equilibrium solubility of H_2, part of the initial hydrate phase has to melt and release H_2 into the aqueous phase. This procedure is far from being arbitrary since it ensures that the hydrate phase is not going to grow along the simulation, and hence, the hydrate phase that remains in the simulation box, once the system has reached equilibrium, has the same occupancy (stoichiometry) as the initial one. This procedure has been recently used by some of the authors of this work to study the three-phase dissociation temperature of the N_2 hydrate when it presents single (1–1) and double (1–2) occupancies.[55]

From the analysis of the density profiles, it is possible to determine not only the H_2 solubility in the aqueous phase but also whether the hydrate phase melts or grows. As has been remarked previously, the initial aqueous phase only contains water molecules, and the only way to reach the equilibrium H_2 solubility is that part of the H_2 hydrate melts. Technically, the H_2 hydrate phase can not grow since there is no H_2 in the initial aqueous phase and an empty hydrate phase is not stable.

https://doi.org/10.1021/acs.energyfuels.5c01012
Energy Fuels 2025, 39, 15184−15197

Table 2. Initial Number of Molecules of Water and H_2 in Each H−L_w Simulation Box at Each H_2 Hydrate Occupancy and Temperature[a]

H_2 hydrate occupancy	T (K)	hydrate phase			L_w phase water
		unit cell	water	H_2	
1−1	250	2 × 2 × 2	1088	192	2176
	260				
	265				
1−2	250	2 × 2 × 2	1088	256	2176
	260				
	265				
	270				
2−2	250	2 × 2 × 2	1088	384	6528
	260				6528
	265				6528
	270				4352
1−3	250	2 × 2 × 2	1088	320	4352
	260				4352
	265				4352
1−4	250	2 × 2 × 2	1088	384	6528
	260				6528
	265				6528
	270				4352

[a]In all cases, the initial L_w phase contains only water molecules.

However, when the occupancy of H_2 molecules in the hydrate is high enough and part of the hydrate melts, it could release into the aqueous phase more H_2 than necessary to reach the solubility of equilibrium, oversaturating the aqueous phase with H_2. This happens as a consequence of the low solubility of H_2 in the aqueous phase and the high amount of H_2 stored in the hydrate structure. When this happens, the hydrate phase grows to take back the excess H_2 from the aqueous phase. If the hydrate phase grows, we can not ensure that the stoichiometry of the new hydrate phase is the same as the initial one and, hence, we can not ensure that the solubility of H_2 in the aqueous phase is reached when the aqueous phase is in contact with a H_2 hydrate phase at only the desire H_2 hydrate occupancy. To avoid oversaturation of the aqueous phase when the H_2 hydrate melts, the number of molecules of water in the initial aqueous phase increases when the occupancy of the H_2 hydrate is increased (see Table 2 for further details). In order to ensure that the stoichiometric of the hydrate along the simulation is the same as the initial seed, we carefully monitor the hydrate phase evolution by the analysis of the density profiles along the simulation. Density profiles provide an accurate description of the system distribution. The peaked shape region of the hydrate density phase contrasts with the flat density region of the fluid phase. By monitoring the length of the hydrate phase, it is possible to determine if the hydrate phase grows, melts, or both at different simulation times. In all cases, the hydrate phase only melts, ensuring that the remaining hydrate phase has the same stoichiometric as the initial seed. At this point, it is also important to mention that there is no diffusion of the guest through the hydrate phase and, as a consequence of this, the only option to modify the initial stoichiometric of the hydrate is the growing of this one with a different occupancy level. Also, it is important to take into account that the H_2 solubility in the aqueous phase in contact via a planar interface with the H_2 hydrate phase increases with the temperature. It means that when the temperature increases, and if the initial aqueous phase is big enough, the H_2 hydrate phase could melt completely in order to reach the equilibrium H_2 solubility value. For this reason, the number of water molecules in the initial aqueous phase is not the same at different temperatures, even when the occupancy of the H_2 hydrate phase is the same (see, for example, the simulation boxes used for 2−2 and 1−4 occupancies in Table 2). Obviously, an increase in the number of molecules involves an increase in the computational effort required to perform the simulations. Hence, the number of water molecules in the aqueous phase is increased only if it is strictly necessary to ensure the stoichiometry of the H_2 hydrate phase.

The H_2 solubility in the aqueous phase is obtained following the same procedure as that in the case of the L_w−L_{H_2} equilibria. First, the density profiles of water and H_2 are obtained from each initial H_2 hydrate occupancy and temperature by dividing the simulation box into 200 slabs along the direction perpendicular to the interface (the z-axis). The center of mass of each molecule is assigned to its corresponding slab, and the mass density profile is obtained by multiplying the molar density profile of each component by its corresponding molar mass. As it has been explained previously, the H_2 solubility in the aqueous phase at each H_2 hydrate occupancy and temperature is obtained by averaging the water and H_2 density profile values of each slab belonging to the aqueous phase. The error bars of the water and H_2 densities in the aqueous phase at each temperature are obtained as the average standard deviation. The H_2 solubility error bars are obtained by propagating the density errors obtained for both components. Again, calculations are performed far enough from the H−L_w interface to avoid any unwanted interfacial effect on the aqueous bulk solubility of H_2. The results obtained in this work for each H_2 hydrate occupancy are presented in Figure 3. As we can see, the solubility of H_2 in the aqueous phase when in contact with a H_2 hydrate phase via a planar interface increases when the temperature is increased. This is the expected behavior when the temperature increases since the hydrate phase becomes less stable and part of it

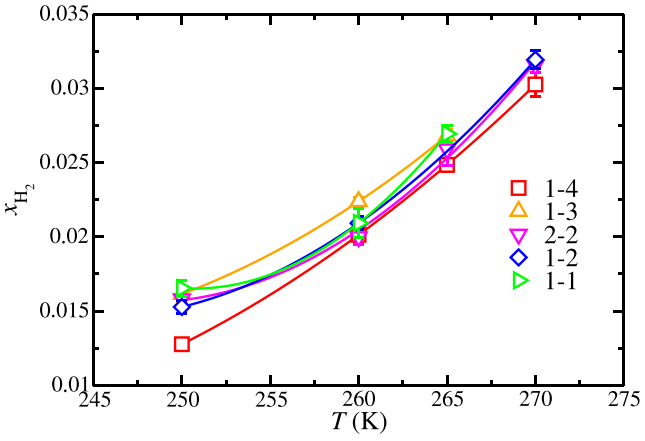

Figure 3. H_2 solubility in the aqueous solution phase as a function of temperature at 185 MPa. The symbols represent the solubility values obtained from the H−L_w *NPT* molecular dynamic simulations performed in this work at different H_2 hydrate occupancies. The meaning of the symbols is given in the legend. Each curve is obtained from the fitting of the solubility value at each occupancy and is included as a guide for the eyes.

https://doi.org/10.1021/acs.energyfuels.5c01012
Energy Fuels 2025, 39, 15184−15197

melts, releasing more H_2 into the aqueous phase. The solubility of H_2 in the aqueous phase, when it is in contact with a hydrate phase, can be understood as a special case of the solubility of a solid in water. Typically, the solubility of a solid in water increases when the temperature increases. In the case of hydrates, the same behavior is expected. However, hydrates are a special case since when part of their structure melts into the aqueous phase, two components are released: water and the guest. Since the solvent is water, the molecules of water from the hydrate become part of the proper solvent of the aqueous solution, while the guest molecules become the solute. As we explained previously, the initial L_w phase is basically a pure water phase, which means that all the H_2 present in this phase comes from the H_2 hydrate phase. It is interesting to remark that the solubility of H_2 in the aqueous phase seems to be almost independent of the H_2 hydrate occupancy since all the systems studied in this work present similar H_2 solubility values. It is also interesting to point out that, in the range of temperatures studied in this work, the H_2 solubility increases linearly when the temperature is increased.

Three-Phase Coexistence Line (T_3) Determination from the Solubility Method. From the analysis of the solubility of H_2 in the aqueous phase obtained from the L_w–L_{H_2} and H–L_w equilibria, it is possible to determine the temperature (T_3) at which the three phases (H–L_w–L_{H_2}) coexist in equilibrium. The T_3 value is obtained as the temperature at which both H_2 solubility curves cross at a certain pressure value. It is also possible to get an estimation of the T_3 error bar by taking into account the error bars of the H_2 solubility values obtained from both (L_w–L_{H_2} and H–L_w) equilibria. Figure 4 shows a representation of the method employed in this work to determine the error bars of the T_3 values. For each equilibrium (L_w–L_{H_2}/H–L_w), three H_2 solubility curves are represented (red/blue). The central one represents the average H_2 solubility value obtained at each temperature, while the upper/lower ones are obtained by summing/resting to the average H_2 solubility value and its corresponding error. As a result, we obtain a central T_3 value which corresponds to the temperature at which the central H_2 solubility curves from both equilibria intersect, a lower T_3^L value obtained as the intersection of the upper and lower H_2 solubility curves obtained from the H–L_w and L_w–L_{H_2} equilibria respectively, and an upper T_3^U value obtained as the intersection of the lower and upper H_2 solubility curves obtained from the H–L_w and L_w–L_{H_2} equilibria respectively. Finally, the T_3 error bar is obtained as $(T_3^U - T_3^L)/2$. The results obtained for each occupancy are collected in Table 3 and the intersections of the solubility curves are presented in Figure 5.

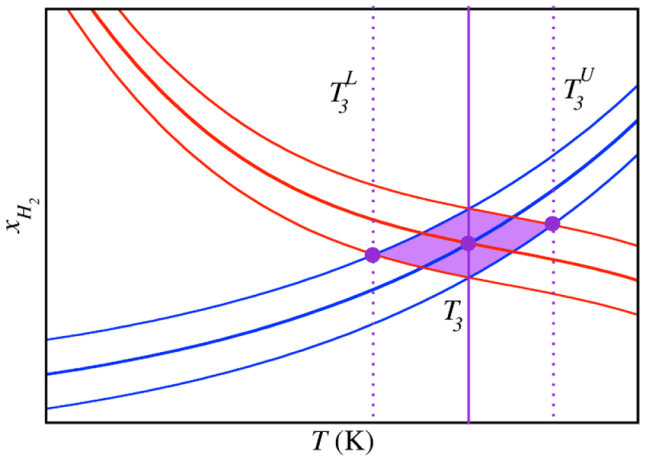

Figure 4. Schematic representation of the determination of the T_3 value and its error bar. The three red and blue curves represent the solubility of H_2 in the aqueous phase as a function of the temperature from the L_w–L_{H_2} and H–L_w equilibria, respectively. In both cases, the central red/blue line represents the equilibrium H_2 solubility, and the upper and lower red/blue lines represent the H_2 solubility error bars. The violet-filled circles represent the lowest (T_3^L), average (T_3), and upper (T_3^U) H_2 solubility and temperature at which the H_2 solubility curves cross.

Table 3. Dissociation Temperature, T_3, of the H_2 Hydrate, at Different H_2 Hydrate Occupancies, as Obtained in This Work Using the Solubility Method at 185 MPa[a]

H_2 hydrate occupancy	T_3 (K)
1–1	264.6(6)
1–2	265.4(7)
2–2	265.6(8)
1–3	264.6(7)
1–4	266.1(8)

[a]Numbers in parentheses indicate the uncertainty of the results.

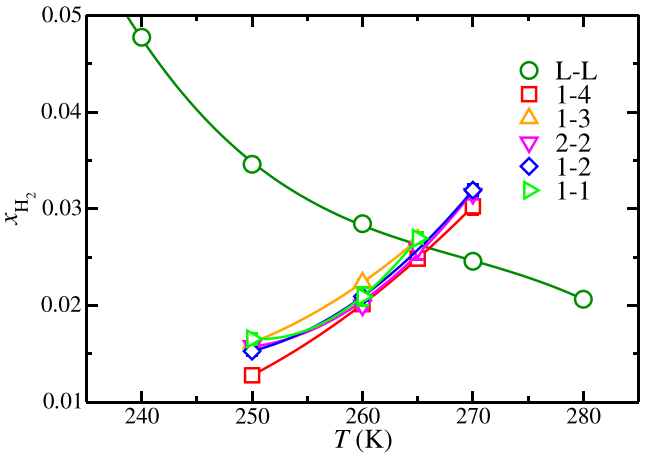

Figure 5. T_3 values obtained at each H_2 hydrate occupancy, as obtained from the solubility method. The meaning of the symbols is shown in the legend and it is the same as in the previous figures. The solubility curves are obtained by fitting the solubility H_2 values in the aqueous phase and are included as a guide for the eyes.

As shown in Figure 5 and Table 3, the H_2 hydrate occupancy has an almost negligible effect on the final T_3 value. All of the T_3 values reported in this work at 185 MPa are the same, within the error bars, independently of the H_2 hydrate occupancy. The T_3 values obtained for each occupancy at 185 MPa are in agreement with that reported by Michalis et al.[18] obtained using the TIP4P/Ice[86] and Feynman–Hibbs (FH)[87] models for water and H_2 molecules, respectively. Although the H_2 model (FH) employed in the original work of Michalis et al.[18] to determine the H_2 hydrate T_3 value is different from the H_2 model used in this work (SG),[57] the same modifying factor of the Berthelot rule (eqs 1 and 2) for the water-H_2 interactions has been employed in both works. This is so since Michalis et al.[18] demonstrated that both H_2

https://doi.org/10.1021/acs.energyfuels.5c01012
Energy Fuels 2025, 39, 15184–15197

(FH and GS) models predict almost the same solubility of H_2 in an aqueous phase, modeled by the TIP4P/Ice water model, when in contact with a pure H_2 phase via a planar interface and the same modification of the Berthelot combining rule is required to match the experimental H_2 solubility results. As well as in the work of Michalis et al.,[18] the T_3 values obtained in this study underestimate the experimental T_3 values by 5−7 K.[21,35] This is the expected result since it is similar to that obtained by Michalis et al.[18] using the same modification of the Berthelot combining rule and the effect of the occupancy of the hydrate on the T_3 value has been demonstrated in this work to be almost negligible.

As we will analyze in the next section, although all the H_2 hydrate occupancies present the same T_3 value, not all of them seem to be equally favored thermodynamically. Technically, it is necessary to calculate the free energy of each hydrate at the three-phase coexistence conditions to analyze which occupancy presents the lowest free-energy value and, hence, which one is the most stable. However, it is possible to estimate which occupancy is the most favored by analyzing the driving force for the nucleation behavior for each H_2 hydrate occupancy. Although the driving force for nucleation represents a difference of free energies and not an absolute free-energy value, it gives us an approximated method to determine which H_2 hydrate occupancy is the most favored under the thermodynamic conditions under which this study was carried out.

Driving Force for Nucleation $\Delta\mu_N^{EC}$. According to the Classical Nucleation Theory (CNT),[88] homogeneous nucleation is an activated process, which means that in order to crystallize the system has to overcome a free-energy barrier. This free-energy barrier depends on the hydrate-aqueous solution's interfacial free energy, γ, and the driving force for nucleation, $\Delta\mu_N$. The driving force for nucleation is defined as the difference between the chemical potential of water and H_2 molecules in the hydrate phase and those in the aqueous solution phase. At the thermodynamic equilibrium conditions of temperature, pressure, and composition, the value of $\Delta\mu_N$ is 0 since the chemical potential of a molecule in each of the phases in equilibrium is the same. In the case of hydrates, the $\Delta\mu_N$ value becomes negative when the aqueous phase is supersaturated with the guest[52,89−93] (H_2 in this case) and when the temperature is below the dissociation temperature.[88,94,95] When $\Delta\mu_N$ becomes more negative, the free-energy barrier that the system has to overcome to crystallize becomes smaller, i.e., it is possible to favor the homogeneous nucleation under supersaturation and/or supercooling conditions.

As we stated in our previous works,[53−55] it is more convenient to express $\Delta\mu_N$ per cage of hydrate formed from the aqueous solution rather per guest molecule when the driving forces for nucleation of hydrates with different occupancies are compared. In previous works, some of the authors of this work presented a general expression for semi/multiple occupied hydrates.[53−55] Following the same approach, the occupancy of the H_2 hydrate is defined as $x_{occ} = n_{H_2}/n_{cg}$, where n_{H_2} and n_{cg} are the number of H_2 molecules and cages per hydrate unit cell, respectively.[53,55] According to Kashchiev and Firoozabadi,[94−96] it is possible to describe the formation of a hydrate molecule from the aqueous solution phase as a chemical reaction at a certain value of P and T. This approach could be generalized to any H_2 hydrate occupancy

$$x_{occ}H_2(aq, x_{H_2}) + 5.67H_2O(aq, x_{H_2}) \rightarrow [(H_2)_{x_{occ}}(H_2O)_{5.67}]_H \quad (3)$$

$H_2(aq,x_{H_2})$ and $H_2O(aq,x_{H_2})$ are the molecules of H_2 and water in the aqueous solution phase with composition x_{H_2}, respectively, while $[(H_2)_{x_{occ}}(H_2O)_{5.67}]_H$ represents a "molecule" of the H_2 hydrate in the solid phase with a certain occupancy, x_{occ}. The 5.67 factor arises because the sII hydrate unit cell is formed by 136 molecules of water and 24 cages, and the "chemical reaction" of the H_2 hydrate formation is reduced according to the number of hydrate cages. The same approach is used to calculate the molar enthalpy of a "hydrate molecule", $\tilde{h}_H = H/N_{cg}$, where H and N_{cg} are the total enthalpy of the H_2 hydrate phase and the number of cages present in the hydrate structure, respectively. Although eq 3 is a general expression and can be applied to any thermodynamic condition, it is particularly interesting to apply this expression along the L_w−L_{H_2} solubility curve, since most of the experiments on the nucleation of hydrates are performed when the water phase is in contact with the guest liquid phase through a planar interface. Following the notation of Grabowska *et al.*,[52] the driving force for nucleation at experimental conditions is denoted as $\Delta\mu_N^{EC}$. Also, it is important to take into account that under experimental conditions the x_{H_2} value of eq 3, at a given P value, is a function of the temperature. In this work, x_{H_2} has been obtained at 185 MPa and different temperatures (see Figure 1).

From eq 3 it is possible to define an approximated but simple method to calculate $\Delta\mu_N^{EC}$.[52−55,94] If eq 3 represents the formation of an H_2 hydrate molecule, the inverse process corresponds to the dissociation of a H_2 hydrate molecule into water and H_2 molecules. Due to the low solubility of H_2 in the aqueous phase, we can assume that the H_2 hydrate molecules dissociate into pure water and H_2. Taking this into account, the dissociation enthalpy of a hydrate molecule, $\tilde{h}_H^{diss}$, is defined as the enthalpy change of the hydrate dissociation in pure water and H_2 molecules. In order to calculate $\Delta\mu_N^{EC}$ in a simple way following the dissociation route approach,[52−55,94] extra approximations have to be taken into account: (1) the solubility of H_2 in the aqueous phase is assumed as 0 independently of the thermodynamic conditions, (2) $\tilde{h}_H^{diss}$ it is calculated at the T_3 value, and (3) it is considered as a constant value independently of the temperature. Taking all these approximations, it is possible to define $\Delta\mu_N^{EC}$ as

$$\Delta\mu_N^{EC}(P, T, x_{occ}) = k_B T \int_{T_3}^{T} \frac{\tilde{h}_H^{diss}(P, T', x_{occ})}{k_B T'^2} dT' \approx -\tilde{h}_H^{diss}(P, T_3, x_{occ})\left(1 - \frac{T}{T_3}\right) \quad (4)$$

Where k_B is the Boltzmann constant. Here it is important to remark that the occupancy of the hydrate is taken into account by the $\tilde{h}_H^{diss}$ value according to eq 3. Equation 4 has been named the dissociation route in our previous works.[52−55]

When the approximations assumed in eq 4 are not undertaken, the expression for the $\Delta\mu_N^{EC}$ calculation becomes more complex since the solubility of H_2 in the aqueous phase has to be explicitly taken into account as well as the change of $\tilde{h}_H^{diss}$ with T and P. As a result, we obtained the following

https://doi.org/10.1021/acs.energyfuels.5c01012
Energy Fuels 2025, 39, 15184−15197

expression named route 1 expression in our previous works[52−55]

$$\frac{\Delta\mu_N^{EC}(P, T, x_{H_2}^{eq}, x_{occ})}{k_BT} = -\int_{T_3}^{T} \frac{\tilde{h}_H^H(P, T', x_{occ}) - \{x_{occ}h_{H_2}(P, T') + 5.67h_{H_2O}(P, T')\}}{k_BT'^2}dT' - 5.67[k_BT\ln\{x_{H_2O}^{eq}(P, T)\} - k_BT_3\ln\{x_{H_2O}^{eq}(P, T_3)\}] \quad (5)$$

Here $\tilde{h}_H^H(P,T',x_{occ})$ represents the enthalpy per cage of the hydrate at P and T' with occupancy x_{occ} and h_{H_2} and h_{H_2O} represent the molar enthalpy of pure H_2 and water, respectively. We refer the reader to our previous works for further details.

Figure 6 shows the $\Delta\mu_N^{EC}$ results obtained by both routes (eqs 5 and 4) as a function of the supercooling degree for the different H_2 hydrate occupancies studied in this work. Although there are quantitative differences between the results obtained by both routes, the qualitative behavior of $\Delta\mu_N^{EC}$ with the supercooling degree and the occupancy is the same. For the same H_2 hydrate occupancy, $\Delta\mu_N^{EC}$ becomes more negative when the supercooling degree is increased. This is the expected result, since the H_2 hydrate phase becomes more stable than the aqueous phase as the temperature decreases. Also, for the same supercooling degree, $\Delta\mu_N^{EC}$ becomes more negative when the amount of H_2 in the H, or large, cages increases from 1 to 3 (from 1 to 1 to 1−3 occupancy), being the 1−3 occupancy of the most favored H_2 hydrate occupancy, closely followed by the 1−2 occupancy. However, if the number of H_2 molecules in the H cages is bigger than 3, then the H_2 hydrate phase becomes slightly less favored and, as a consequence, $\Delta\mu_N^{EC}$ increases becoming more positive. These results are in good agreement with those reported previously in the literature where the occupancy of the D and H cages of the H_2 hydrate was studied from Monte Carlo[17,25,30,32] and molecular dynamic[29] simulations. In Figure 6 we can see that the $\Delta\mu_N^{EC}$ results obtained, from both routes, for the 1−4 occupancy are between those obtained for the 1−1 and 1−2 occupancies. Also, we can state from Figure 6 that the double occupancy of the D, or small, cages destabilizes the hydrate structure due to the high repulsion present when two H_2 molecules are confined in the D cages. As a consequence, the $\Delta\mu_N^{EC}$ values obtained for the 2−2 occupancy are the most positive ones, revealing that among the different occupancies studied in this work, the 2−2 occupancy seems to be the less favored one. When considering hydrates as potential gas storage materials, the number of H_2 molecules per cage is a crucial factor in determining the storage capacity of a given hydrate structure. Experimentally, it is known that the sII hydrate small cages could host two H_2 molecules, while large cages could store up to four H_2 molecules,[19] leading to a total H_2 storage capacity of 5.0 wt % for H_2 hydrates. This H_2 storage capacity is close to the US DOE 5.5 wt % target for 2025. However, our results indicate that the most stable hydrate configuration consists of three H_2 molecules in the large cages and only one H_2 molecule in the small one. This H_2 hydrate stoichiometric results in a storage capacity of 3.2 wt %, which is roughly bigger than half of the US DOE ultimate target.

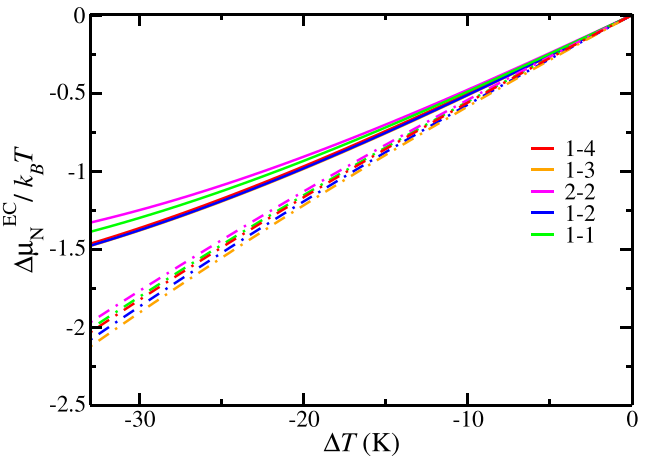

Figure 6. $\Delta\mu_N^{EC}$ values for each H_2 hydrate occupancy studied in this work as a function of the supercooling degree at 185 MPa. Continuous and dashed lines represent the results obtained by eqs 5 and 4 respectively.

Effect of the Temperature and Occupancy on Unit-Cell Size. From the bulk simulations of the H_2 hydrate phase used to determine the $\Delta\mu_N^{EC}$, we analyze the average unit-cell size or lattice constant, a as a function of the temperature and the occupancy of the H_2 hydrate phase at 185 MPa. Due to the cubic symmetry of the sII hydrate structure, we obtain a as the cubic root of the average volume of the hydrate unit cell. As shown in Figure 7, the H_2 hydrate lattice constant increases when the temperature is increased, although the dependency of a with the temperature is almost negligible. This is an expected result since the same behavior was observed by some of the authors of this work for the case of the N_2 hydrate.[55] It is also interesting to analyze the behavior of a with H_2 occupancy. As shown in Figure 7, a increases when the occupancy is increased. This is an expected behavior since a larger a value allows better accommodation of the H_2 molecules inside the hydrate structure. As we can see, when the H_2 occupancy increases from 1 H_2 molecule in the H, or large, cages to 4 (i.e., from the 1−1 to 1−4 occupancies), the a value is increased by ≈0.7% in all the range of temperatures. It is also interesting to observe that when the D, or small, and the H, or large, cages are doubly occupied (2−2 occupancy), the a value is higher

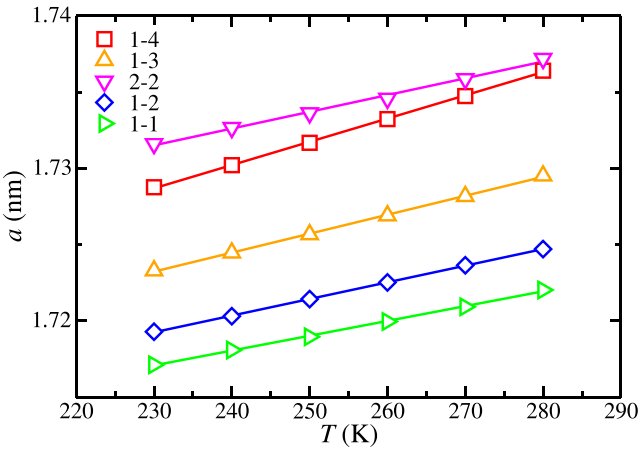

Figure 7. Average unit-cell size or lattice constant (a) obtained from MD *NPT* bulk simulations of the H_2 hydrate phase as a function of T and the occupancy at 185 MPa. The meaning of the symbols is shown in the legend, and it is the same as in previous figures. The lines are included as a guide for the eyes.

https://doi.org/10.1021/acs.energyfuels.5c01012
Energy Fuels 2025, 39, 15184−15197

than in the 1−4 occupancy even when the total number of H_2 molecules in the H_2 hydrate unit cell is the same for both occupancies (48 H_2 molecules). This is because the repulsion provoked by 2 H_2 molecules encapsulated in the small D and large H cages is larger than the repulsion provoked by 4 H_2 molecules in the large H cages and 1 H_2 molecule in the small D cages.

Direct Coexistence Method. Finally, we study the three-phase coexistence temperature, T_3, using a direct coexistence method. Following this methodology, the three phases involved in the equilibrium are placed together in the same simulation box. As has been explained previously, at a given pressure value, two different behaviors are shown as a function of the temperature. If the temperature is above the T_3 value, then the H_2 hydrate phase is unstable and melts, evolving the three-phase system to a two-phase L_w−L_{H_2} equilibrium. Contrarily, if the temperature is below the T_3 value, the H_2 hydrate phase grows until extinguishing the aqueous or guest phase depending on the initial amount of molecules of water and guest in both phases. To determine whether the H_2 hydrate phase grows or melts, the potential energy of the system is monitored as a function of time. When the H_2 hydrate phase grows, new hydrogen bonds are created, and the potential energy decreases. On the contrary, when the H_2 hydrate phase melts, the potential energy increases as a function of time. The T_3 is placed between the highest temperature at which the hydrate phase grows and the lowest temperature at which it melts.

In this work, the initial configuration box is built up, putting in contact the three phases, H_2 hydrate, aqueous, and pure H_2. The initial sII H_2 hydrate phase is built as explained in H−L_w Equilibria: Solubility of H_2 in Liquid Water When It Is in Contact with H_2 Hydrate section. Particularly, it is formed by a 2 × 2 × 2 unit cell with 1−3 H_2 occupancy for the hydrate phase in contact with an aqueous phase with 1088 water molecules and with an H_2 phase with 600 H_2 molecules. Due to the use of periodic boundary conditions, this arrangement ensures that the three phases are in contact, with one of the phases surrounded by the other two. We choose the 1−3 occupancy since it has been shown that with the most negative values of $\Delta\mu_N^{EC}$ as a function of the supercooling degree at 185 MPa. As we explained previously, this means that the 1−3 occupancy, from a thermodynamic point of view, is the most favored stoichiometry. Simulations were carried out at 100, 185, and 300 MPa and at different temperatures. As it has been explained in Section II, we propose in this work an extra parameter, b_0, for the Berthelot modified combination rule (see eq 2) proposed by Michalis et al.[18] in order to improve the predictions of the T_3 values in the 100−300 MPa pressure range. Although the modified factor, χ, proposed by Michalis et al.[18] gives an excellent prediction of the H_2 solubility in water and improves the T_3 predictions, the T_3 values obtained still underestimate the experimental results reported in the literature[21,35] by 5−7 K.

Figure 8 shows the potential energy results obtained at 100, 185, and 300 MPa and at different temperatures. From the results presented in Figure 8 and following the procedure explained previously, it is easy to determine that 263(1), 270(1), and 273(1) K are the T_3 values obtained at 100, 185, and 300 MPa, respectively. As can be seen in Table 4 and Figure 9, the results obtained in this work using the direct coexistence technique and the additional b_0 parameter in eq 2

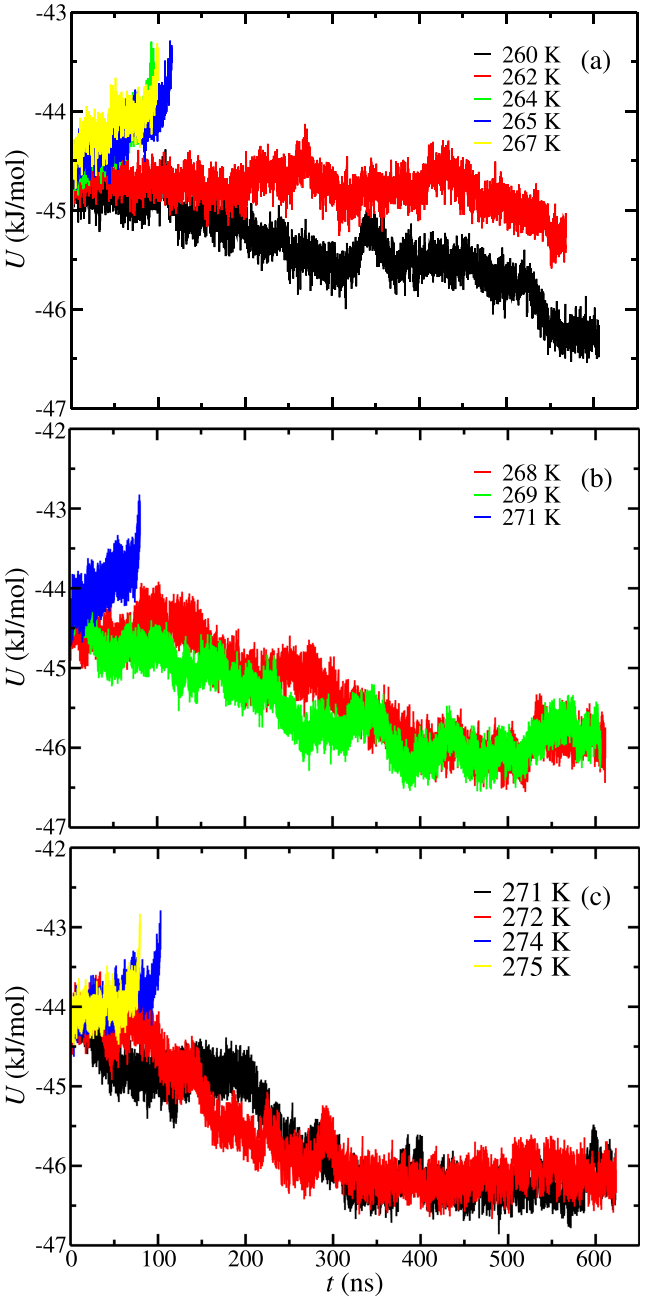

Figure 8. Potential energy as a function of time as obtained from *NPT* molecular dynamic simulations at different temperatures and pressures. (a)−(c) Correspond to results obtained at 100, 185, and 300 MPa, respectively. In all cases, the initial H_2 hydrate phase contains 1 H_2 molecules in the small D cages and 3 H_2 molecules in the large H cages (1−3 occupancy).

Table 4. Dissociation Temperature of the H_2 Hydrate Obtained in This Work from the Direct Coexistence Technique (T_3^{DC})[a]

P (MPa)	T_3^{DC} (K)	T_3^{EXP} (K)
100	263(1)	264.1
185	270(1)	269.9/271.6
300	273(1)	274.6

[a]Results from the experimental data reported in the literature[21,35] (T_3^{EXP}) are also shown.

https://doi.org/10.1021/acs.energyfuels.5c01012
Energy Fuels 2025, 39, 15184−15197

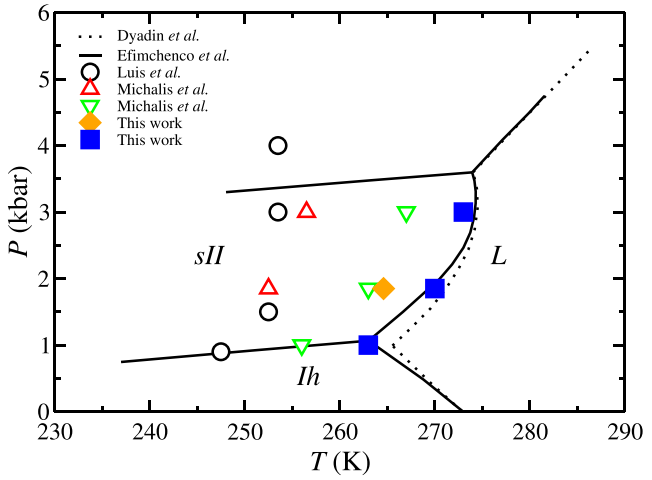

Figure 9. H_2 hydrate phase diagram. The sII, I_h, and L regions stand for sII H_2 hydrate, hexagonal ice, and liquid water, respectively. Continuous and dotted black lines correspond to the experimental data reported by Efimchenco et al.[35] and Dyadin et al.[21] respectively. Open symbols correspond to the simulation predictions of the three-phase coexistence line reported in the literature by Luis et al.[68] (black circles) and Michalis et al.[18] (red up and green down triangles). Finally, filled symbols correspond to the three-phase coexistence conditions obtained in this work. The filled orange represents the predictions obtained by the solubility method at 185 MPa and using the 1−3 occupancy and the original combining rules proposed by Michalis et al.[18] (i.e., $b_0 = 0$ in eq 2). Finally, the filled blue squares correspond to the predictions obtained in this work using the direct coexistence technique and the extra parameter $b_0 = 0.1$ with 1−3 H_2 hydrate occupancy.

are equal, within the error bars, to the experimental data reported in the literature.[21,35] It is also interesting to remark that the result obtained by the solubility method for the 1−3 H_2 hydrate occupancy is very close to the experimental data, slightly underestimating the experimental T_3 value at the same time that provides an accurate estimation of the H_2 solubility value in an aqueous phase. On the other hand, the addition of the b_0 parameter in eq 2 improves the prediction of the T_3 values but the H_2 solubility in an aqueous phase is slightly overestimated.[18] At this point, it is up to the lector to prioritize the prediction of the T_3 or the H_2 solubility by taking into account or not the b_0 parameter in eq 2. In both cases, the results obtained by both modified combining rules are excellent.

CONCLUSIONS

In this work, we determined the three-phase $H-L_w-L_{H_2}$ coexistence line following two different molecular computer simulation methods. In both methods, the water and H_2 molecules are described using the TIP4P/Ice[56] and a modified version of the SG model[18,29,57] respectively. In both cases, the Berthelot combination rule for the water-H_2 interactions has been modified to improve the H_2 solubility and the T_3 predictions. First, we study the effect of the H_2 hydrate occupancy on the T_3 value at 185 MPa using the solubility method and 5 different H_2 hydrate occupancies (1−1, 1−2, 2−2, 1−3, and 1−4). We use the same modification of the Berthelot combining rule proposed by Michalis et al.,[18] which provides an accurate estimation of the H_2 solubility in an aqueous phase but slightly underestimates the T_3 value. From this analysis, we conclude that the effect of the H_2 hydrate occupancy on the T_3 value is negligible since all the occupancies considered in this work provide almost the same T_3 result. The T_3 values obtained following this procedure are in very good agreement with the experimental data reported in the literature[21,35] although they are slightly underestimated.

We also estimate the driving force for nucleation, $\Delta\mu_N^{EC}$, of the H_2 hydrate as a function of the supercooling degree for the five different occupancies considered in this work. We find that multiple occupancy of the large H cages is favored in general, becoming $\Delta\mu_N^{EC}$ more negative when the occupancy is increased from 1 to 4 H_2 molecules, reaching the most negative value when the H cages are occupied by 3 H_2 molecules while the small D cages are single occupied. We also find that the double occupancy of the D and H cages is not favored, becoming $\Delta\mu_N^{EC}$ more positive than that when both cages are singly occupied. This is due to the high repulsion suffered by both H_2 molecules encapsulated inside the small D cages. To the best of our knowledge, this is the first time that the effect of the occupancy on the dissociation temperature and the driving force for nucleation of the H_2 hydrate have been determined from computer simulations.

Finally, we study the dissociation temperature at three different pressures (100, 185, and 300 MPa) by using the direct coexistence technique. We perform the simulations with an initial 1−3 H_2 hydrate phase and, in order to improve the T_3 predictions, we propose a new modification of the Berthelot combining rule for the water−H_2 cross-interaction. The results obtained with this new combining rule modification are in excellent agreement with the experimental results reported in the literature.[21,35]

ASSOCIATED CONTENT

Data Availability Statement

The data that support the findings of this study are available within the article.

AUTHOR INFORMATION

Corresponding Authors

Maria M. Conde − *Departamento de Ingeniería Química Industrial y del Medio Ambiente, Escuela Técnica Superior de Ingenieros Industriales, Universidad Politécnica de Madrid, 28006 Madrid, Spain;* orcid.org/0000-0003-2822-9141; Email: maria.mconde@upm.es

Felipe J. Blas − *Laboratorio de Simulación Molecular y Química Computacional, CIQSO-Centro de Investigación en Química Sostenible and Departamento de Ciencias Integradas, Universidad de Huelva, 21006 Huelva, Spain;* orcid.org/0000-0001-9030-040X; Email: felipe@uhu.es

Authors

Miguel J. Torrejón − *Laboratorio de Simulación Molecular y Química Computacional, CIQSO-Centro de Investigación en Química Sostenible and Departamento de Ciencias Integradas, Universidad de Huelva, 21006 Huelva, Spain;* orcid.org/0009-0002-0470-2002

Samuel Blazquez − *Departamento de Química Física I, Fac. Ciencias Químicas, Universidad Complutense de Madrid, 28040 Madrid, Spain;* orcid.org/0000-0002-6218-3880

Jesús Algaba − *Laboratorio de Simulación Molecular y Química Computacional, CIQSO-Centro de Investigación en Química Sostenible and Departamento de Ciencias Integradas, Universidad de Huelva, 21006 Huelva, Spain;* orcid.org/0000-0001-8371-5287

https://doi.org/10.1021/acs.energyfuels.5c01012
Energy Fuels 2025, 39, 15184−15197

Complete contact information is available at:
https://pubs.acs.org/10.1021/acs.energyfuels.5c01012

Notes

The authors declare no competing financial interest.

■ ACKNOWLEDGMENTS

The authors wish to express their sincere gratitude to Dr. E. Dendy Sloan for his invaluable contributions to the study of gas hydrates. His pioneering work has not only been fundamental in advancing experimental knowledge of hydrates but has also opened new doors to molecular simulation in this field, enabling a deeper understanding of their structure and behavior. His legacy continues to guide both theoretical and applied research, inspiring future generations of scientists. We deeply appreciate his tireless dedication and the lasting impact of his contributions to both academia and industry. M.J.T., J.A., and F.J.B. acknowledge grant refs (PID2021-125081NB-I00 and PID2024-158030NB-I00) financed both by MCIN/AEI/10.13039/501100011033 and FEDER EU, and Universidad de Huelva (P.O. FEDER EPIT1282023), also cofinanced by EU FEDER funds. S.B. and M.M.C. also acknowledge grant ref PID2022-136919NB-C32 financed by MCIN/AEI/10.13039/501100011033 and FEDER EU. M.J.T. acknowledges the research contract (ref 01/2022/38143) of Programa Investigo (Plan de Recuperación, Transformación y Resiliencia, Fondos NextGeneration EU) from Junta de Andalucía (HU/INV/0004/2022). We also greatly acknowledge RES resources provided by the Barcelona Supercomputing Center in Mare Nostrum to FI-2023-3-0011 and by The Supercomputing and Bioinnovation Center of the University of Malaga in Picasso to FI-2024-1-0017. S.B. acknowledges Ayuntamiento de Madrid for a Residencia de Estudiantes grant. The authors gratefully acknowledge the Universidad Politecnica de Madrid (www.upm.es) for providing computing resources on the Magerit Supercomputer.

■ REFERENCES

(1) Sloan, E. D.; Koh, C. *Clathrate Hydrates of Natural Gases*, 3rd ed.; CRC Press: New York, 2007.
(2) Ripmeester, J. A.; Alavi, S. *Clathrate Hydrates: Molecular Science and Characterization*; Wiley-VCH: Weinheim, Germany, 2022.
(3) Ma, Z.; Zhang, P.; Bao, H.; Deng, S. Review of fundamental properties of CO_2 hydrates and CO_2 capture and separation using hydration method. *Renewable Sustainable Energy Rev.* **2016**, *53*, 1273−1302.
(4) Conde, M. M.; Torré, J. P.; Miqueu, C. Revisiting the thermodynamic modelling of type I gas-hydroquinone clathrates. *Phys. Chem. Chem. Phys.* **2016**, *18*, 10018−10027.
(5) Dashti, H.; Yew, L. Z.; Lou, X. Recent advances in gas hydrate-based CO_2 capture. *J. Nat. Gas Sci. Eng.* **2015**, *23*, 195−207.
(6) Cannone, S. F.; Lanzini, A.; Santarelli, M. A review on CO_2 capture technologies with focus on CO_2-enhanced methane recovery from hydrates. *Energies* **2021**, *14*, 387.
(7) Duc, N. H.; Chauvy, F.; Herri, J.-M. CO_2 capture by hydrate crystallization-A potential solution for gas emission of steelmaking industry. *Energy Convers. Manage.* **2007**, *48*, 1313−1322.
(8) Choi, W.; Mok, J.; Lee, J.; Lee, Y.; Lee, J.; Sum, A. K.; Seo, Y. Effective CH_4 production and novel CO_2 storage through depressurization-assisted replacement in natural gas hydrate-bearing sediment. *Appl. Energy* **2022**, *326*, 119971.
(9) Lee, B. R.; Koh, C. A.; Sum, A. K. Quantitative measurement and mechanisms for CH_4 production from hydrates with the injection of liquid CO_2. *Phys. Chem. Chem. Phys.* **2014**, *16*, 14922−14927.
(10) Mi, F.; Li, W.; Pang, J.; Moultos, O. A.; Ning, F.; Vlugt, T. J. Molecular insights into the microscopic behavior of CO_2 hydrates in oceanic sediments: Implications for carbon sequestration. *J. Phys. Chem. C* **2024**, *128*, 18588−18597.
(11) Yi, L.; Zhou, X.; He, Y.; Cai, Z.; Zhao, L.; Zhang, W.; Shao, Y. Molecular Dynamics Simulation Study on the Growth of Structure II Nitrogen Hydrate. *J. Phys. Chem. B* **2019**, *123*, 9180−9186.
(12) Hassanpouryouzband, A.; Yang, J.; Tohidi, B.; Chuvilin, E.; Istomin, V.; Bukhanov, B.; Cheremisin, A. CO_2 capture by injection of flue gas or CO_2-N_2 mixtures into hydrate reservoirs: Dependence of CO_2 capture efficiency on gas hydrate reservoir conditions. *Environ. Sci. Technol.* **2018**, *52*, 4324−4330.
(13) Chong, Z. R.; Yang, S. H. B.; Babu, P.; Linga, P.; Li, X.-S. Review of natural gas hydrates as an energy resource: Prospects and challenges. *Appl. Energy* **2016**, *162*, 1633−1652.
(14) Zheng, J.; Chong, Z. R.; Qureshi, M. F.; Linga, P. Carbon dioxide sequestration via gas hydrates: a potential pathway toward decarbonization. *Energy Fuels* **2020**, *34*, 10529−10546.
(15) Bourry, C.; Charlou, J.-L.; Donval, J.-P.; Brunelli, M.; Focsa, C.; Chazallon, B. X-ray synchrotron diffraction study of natural gas hydrates from African margin *Geophys. Res. Lett.* 2007, *34*, L22303.
(16) Tsimpanogiannis, I. N.; Economou, I. G. Monte Carlo simulation studies of clathrate hydrates: A review. *J. Supercrit. Fluids* **2018**, *134*, 51−60.
(17) Brumby, P. E.; Yuhara, D.; Hasegawa, T.; Wu, D. T.; Sum, A. K.; Yasuoka, K. Cage occupancies, lattice constants, and guest chemical potentials for structure II hydrogen clathrate hydrate from Gibbs ensemble Monte Carlo simulations. *J. Chem. Phys.* **2019**, *150*, 134503.
(18) Michalis, V. K.; Economou, I. G.; Stubos, A. K.; Tsimpanogiannis, I. N. Phase equilibria molecular simulations of hydrogen hydrates via the direct phase coexistence approach. *J. Chem. Phys.* **2022**, *157*, 154501.
(19) Mao, W. L.; Mao, H. K.; Goncharov, A. F.; Struzhkin, V. V.; Guo, Q.; Hu, J.; Shu, J.; Hemley, R. J.; Somayazulu, M.; Zhao, Y. Hydrogen Clusters in Clathrate Hydrate. *Science* **2002**, *297*, 2247−2249.
(20) Belosudov, R. V.; Bozhko, Y. Y.; Zhdanov, R. K.; Subbotin, O. S.; Kawazoe, Y.; Belosludov, V. R. Hydrogen hydrates: Equation of state and self-preservation effect. *Fluid Phase Equilib.* **2016**, *413*, 220−228.
(21) Dyadin, Y. A.; Larionov, E. G.; Manakov, A. Y.; Zhurko, F. V.; Aladko, E. Y.; Mikina, T. V.; Komarov, V. Y. Clathrate hydrates of hydrogen and neon. *Mendeleev Commun.* **1999**, *9*, 209−210.
(22) Dyadin, Y. A.; Larionov, E.; Aladko, E. Y.; Manakov, A. Y.; Zhurko, F.; Mikina, T.; Komarov, V. Y.; Grachev, E. Clathrate formation in water-noble gas (hydrogen) systems at high pressures. *J. Struct. Chem.* **1999**, *40*, 790−795.
(23) Grim, R. G.; Kerkar, P. B.; Shebowich, M.; Arias, M.; Sloan, E. D.; Koh, C. A.; Sum, A. K. Synthesis and characterization of sI clathrate hydrates containing hydrogen. *J. Phys. Chem. C* **2012**, *116*, 18557−18563.
(24) Mao, W. L.; Mao, H. K. Hydrogen Storage in Molecular Compounds. *Proc. Natl. Acad. Sci. U.S.A.* **2004**, *101*, 708−710.
(25) Katsumasa, K.; Koga, K.; Tanaka, H. On the thermodynamic stability of hydrogen clathrate hydrates. *J. Chem. Phys.* **2007**, *127*, 044509.
(26) Papadimitriou, N. I.; Tsimpanogiannis, I. N.; Economou, I. G.; Stubos, A. K. The effect of lattice constant on the storage capacity of hydrogen hydrates: A Monte Carlo study. *Mol. Phys.* **2016**, *114*, 2664−2671.
(27) Liu, J.; Hou, J.; Xu, J.; Liu, H.; Chen, G.; Zhang, J. Ab initio study of the molecular hydrogen occupancy in pure H_2 and binary H_2-THF clathrate hydrates. *J. Hydrogen Energy* **2017**, *42*, 17136−17143.
(28) Belosludov, R. V.; Subbotin, O. S.; Mizuseki, H.; Kawazoe, Y.; Belosludov, V. R. Accurate description of phase diagram of clathrate hydrates at the molecular level. *J. Chem. Phys.* **2009**, *131*, 244510.

(29) Alavi, S.; Ripmeester, J. A.; Klug, D. D. Molecular-dynamics study of structure II hydrogen clathrates. *J. Chem. Phys.* **2005**, *123*, 024507.
(30) Papadimitriou, N. I.; Tsimpanogiannis, I.; Papaioannou, A. T.; Stubos, A. Evaluation of the hydrogen-storage capacity of pure H_2 and binary H_2-THF hydrates with Monte Carlo simulations. *J. Phys. Chem. C* **2008**, *112*, 10294−10302.
(31) Papadimitriou, N. I.; Tsimpanogiannis, I.; Peters, C.; Papaioannou, A. T.; Stubos, A. Hydrogen storage in sH hydrates: A Monte Carlo study. *J. Phys. Chem. B* **2008**, *112*, 14206−14211.
(32) Chun, D.-H.; Lee, T.-Y. Molecular simulation of cage occupancy and selectivity of binary THF-H_2 sII hydrate. *Mol. Simul.* **2008**, *34*, 837−844.
(33) Papadimitriou, N. I.; Tsimpanogiannis, I. N.; Economou, I. G.; Stubos, A. K. Storage of H_2 in clathrate hydrates: Evaluation of different force-fields used in Monte Carlo simulations. *Mol. Phys.* **2017**, *115*, 1274−1285.
(34) Brumby, P. E.; Yuhara, D.; Wu, D. T.; Sum, A. K.; Yasuoka, K. Cage occupancy of methane hydrates from Gibbs ensemble Monte Carlo simulations. *Fluid Phase Equilib.* **2016**, *413*, 242−248.
(35) Efimchenko, V. S.; Antonov, V.; Barkalov, O.; Klyamkin, S.; Tkacz, M. Two triple points in the H_2O-H_2 system. *High Pressure Res.* **2009**, *29*, 250−253.
(36) Zhang, J.; Li, Y.; Yin, Z.; Zheng, X. Y.; Linga, P. How THF tunes the kinetics of H2-THF hydrates? A kinetic study with morphology and calorimetric analysis. *Ind. Eng. Chem. Res.* **2023**, *62*, 21918−21932.
(37) Zhang, J.; Li, Y.; Yin, Z.; Linga, P.; He, T.; Zheng, X. Y. Coupling amino acid L-Val with THF for superior hydrogen hydrate kinetics: Implication for hydrate-based hydrogen storage. *Chem. Eng. J.* **2023**, *467*, 143459.
(38) Zhang, J.; Li, Y.; Rao, Y.; Li, Y.; He, T.; Linga, P.; Wang, X.; Chen, Q.; Yin, Z. Probing the pathway of H2-THF and H2-DIOX sII hydrates formation: Implication on hydrate-based H2 storage. *Appl. Energy* **2024**, *376*, 124289.
(39) Asadi, M.; Peyvandi, K.; Varaminian, F.; Mokarian, Z. Investigation of THF hydrate formation kinetics: Experimental measurements of volume changes. *J. Mol. Liq.* **2019**, *290*, 111200.
(40) Sun, S.; Peng, X.; Zhang, Y.; Zhao, J.; Kong, Y. Stochastic nature of nucleation and growth kinetics of THF hydrate. *J. Chem. Thermodyn.* **2017**, *107*, 141−152.
(41) Suzuki, T.; Muraoka, M.; Nagashima, K. Foreign particle behavior at the growth interface of tetrahydrofuran clathrate hydrates. *J. Cryst. Growth* **2011**, *318*, 131−134.
(42) Sabase, Y.; Nagashima, K. Growth mode transition of tetrahydrofuran clathrate hydrates in the guest/host concentration boundary layer. *J. Phys. Chem. B* **2009**, *113*, 15304−15311.
(43) Strauch, B.; Schicks, J. M.; Luzi-Helbing, M.; Naumann, R.; Herbst, M. The difference between aspired and acquired hydrate volumes-A laboratory study of THF hydrate formation in dependence on initial THF: H_2O ratios. *J. Chem. Thermodyn.* **2018**, *117*, 193−204.
(44) Ganji, H.; Manteghian, M.; Zadeh, K. S. A kinetic study on tetrahydrofuran hydrate crystallization. *J. Chem. Eng. Jpn.* **2006**, *39*, 401−408.
(45) Andersson, O.; Suga, H. Thermal conductivity of normal and deuterated tetrahydrofuran clathrate hydrates. *J. Phys. Chem. Solids* **1996**, *57*, 125−132.
(46) Kumar, A.; Maini, B.; Bishnoi, P.; Clarke, M.; Zatsepina, O.; Srinivasan, S. Experimental determination of permeability in the presence of hydrates and its effect on the dissociation characteristics of gas hydrates in porous media. *J. Pet. Sci. Eng.* **2010**, *70*, 114−122.
(47) Makino, T.; Sugahara, T.; Ohgaki, K. Stability Boundaries of Tetrahydrofuran + Water System. *J. Chem. Eng. Data* **2005**, *50*, 2058−2060.
(48) Algaba, J.; Romero-Guzmán, C.; Torrejón, M. J.; Blas, F. J. Prediction of the univariant two-phase coexistence line of the tetrahydrofuran hydrate from computer simulation. *J. Phys. Chem. A* **2024**, *160*, 164718.
(49) Torrejón, M. J.; Romero-Guzmán, C.; Piñeiro, M. M.; Blas, F. J.; Algaba, J. Simulation of the THF hydrate - water interfacial free energy from computer simulation. *J. Chem. Phys.* **2024**, *161*, 064701.
(50) Torré, J.-P.; Haillot, D.; Rigal, S.; de Souza Lima, R.; Dicharry, C.; Bedecarrats, J.-P. 1, 3 Dioxolane versus tetrahydrofuran as promoters for CO_2-hydrate formation: Thermodynamics properties, and kinetics in presence of sodium dodecyl sulfate. *Chem. Eng. Sci.* **2015**, *126*, 688−697.
(51) Tanaka, H.; Yagasaki, T.; Matsumoto, M. On the thermodynamic stability of clathrate hydrates VI: complete phase diagram. *J. Phys. Chem. B* **2018**, *122*, 297−308.
(52) Grabowska, J.; Blázquez, S.; Sanz, E.; Zerón, I. M.; Algaba, J.; Míguez, J. M.; Blas, F. J.; Vega, C. Solubility of methane in water: some useful results for hydrate nucleation. *J. Phys. Chem. B* **2022**, *126*, 8553−8570.
(53) Algaba, J.; Zerón, I. M.; Míguez, J. M.; Grabowska, J.; Blazquez, S.; Sanz, E.; Vega, C.; Blas, F. J. Solubility of carbon dioxide in water: Some useful results for hydrate nucleation. *J. Chem. Phys.* **2023**, *158*, 054505.
(54) Algaba, J.; Torrejón, M. J.; Blas, F. J. Dissociation line and driving force for nucleation of the nitrogen hydrate from computer simulation. *J. Chem. Phys.* **2023**, *159*, 224707.
(55) Torrejón, M. J.; Algaba, J.; Blas, F. J. Dissociation line and driving force for nucleation of the nitrogen hydrate from computer simulation. II. Effect of multiple occupancy. *J. Chem. Phys.* **2024**, *161*, 054712.
(56) Abascal, J. L. F.; Sanz, E.; Fernández, R. G.; Vega, C. A Potential Model for the Study of Ices and Amorphous Water: TIP4P/Ice. *J. Chem. Phys.* **2005**, *122*, 234511.
(57) Silvera, I. F.; Goldman, V. V. The isotropic intermolecular potential for H_2 and D_2 in the solid and gas phases. *J. Chem. Phys.* **1978**, *69*, 4209−4213.
(58) Conde, M. M.; Vega, C. Determining the three-phase coexistence line in methane hydrates using computer simulations. *J. Chem. Phys.* **2010**, *133*, 064507.
(59) Conde, M. M.; Vega, C. Note: A simple correlation to locate the three phase coexistence line in methane-hydrate simulations. *J. Chem. Phys.* **2013**, *138*, 056101.
(60) Michalis, V. K.; Costandy, J.; Tsimpanogiannis, I. N.; Stubos, A. K.; Economou, I. G. Prediction of the phase equilibria of methane hydrates using the direct phase coexistence methodology. *J. Chem. Phys.* **2015**, *142*, 044501.
(61) Míguez, J. M.; Conde, M. M.; Torré, J.-P.; Blas, F. J.; Piñeiro, M. M.; Vega, C. Molecular Dynamics Simulation of CO_2 Hydrates: Prediction of Three Phase Coexistence Line. *J. Chem. Phys.* **2015**, *142*, 124505.
(62) Costandy, J.; Michalis, V. K.; Tsimpanogiannis, I. N.; Stubos, A. K.; Economou, I. G. The role of intermolecular interactions in the prediction of the phase equilibria of carbon dioxide hydrates. *J. Chem. Phys.* **2015**, *143*, 094506.
(63) Pérez-Rodríguez, M.; Vidal-Vidal, A.; Míguez, J.; Blas, F. J.; Torré, J.-P.; Piñeiro, M. M. Computational study of the interplay between intermolecular interactions and CO_2 orientations in type I hydrates. *Phys. Chem. Chem. Phys.* **2017**, *19*, 3384−3393.
(64) Fernández-Fernández, A.; Pérez-Rodríguez, M.; Comesaña, A.; Piñeiro, M. M. Three-phase equilibrium curve shift for methane hydrate in oceanic conditions calculated from Molecular Dynamics simulations. *J. Mol. Liq.* **2019**, *274*, 426−433.
(65) Blazquez, S.; Vega, C.; Conde, M. M. Three phase equilibria of the methane hydrate in NaCl solutions: A simulation study. *J. Mol. Liq.* **2023**, *383*, 122031.
(66) Borrero, A.; Díaz-Acosta, A.; Blazquez, S.; Zerón, I.; Algaba, J.; Conde, M.; Blas, F. Three-Phase Equilibria of CO_2 Hydrate from Computer Simulation in the Presence of NaCl. *Energy Fuels* **2025**, *39*, 5522−5533.
(67) van der Spoel, D.; Lindahl, E.; Hess, B.; Groenhof, G.; Mark, A. E.; Berendsen, H. J. GROMACS: Fast, Flexible, and Free. *J. Comput. Chem.* **2005**, *26*, 1701−1718.

(68) Luis, D. P.; Romero-Ramirez, I.; González-Calderón, A.; López-Lemus, J. The coexistence temperature of hydrogen clathrates: A molecular dynamics study. *J. Chem. Phys.* **2018**, *148*, 114503.
(69) Cuendet, M. A.; Gunsteren, W. F. V. On the Calculation of Velocity-Dependent Properties in Molecular Dynamics Simulations Using the Leapfrog Integration Algorithm. *J. Chem. Phys.* **2007**, *127*, 184102.
(70) Nosé, S. A Molecular Dynamics Method for Simulations in the Canonical Ensemble. *Mol. Phys.* **1984**, *52*, 255−268.
(71) Parrinello, M.; Rahman, A. Polymorphic Transitions in Single Crystals: A New Molecular Dynamics Method. *J. Appl. Phys.* **1981**, *52*, 7182−7190.
(72) Essmann, U.; Perera, L.; Berkowitz, M. L.; Darden, T.; Lee, H.; Pedersen, L. G. A Smooth Particle Mesh Ewald method. *J. Chem. Phys.* **1995**, *103*, 8577−8593.
(73) Ladd, J. C.; Woodcock, L. V. Triple-point coexistence properties of the Lennard-Jones system. *Chem. Phys. Lett.* **1977**, *51*, 159155.
(74) Vega, C.; Sanz, E.; Abacal, J. L. F.; Noya, E. G. Determination of phase diagrams via computer simulation: Methodology and applications to water, electrolytes and proteins. *J. Phys.: Condensed Matter* **2008**, *20*, 153101.
(75) Zhang, Z.; Kusalik, P. G.; Wu, N.; Liu, C.; Zhang, Y. Molecular simulation study on the stability of methane hydrate confined in slit-shaped pores. *Energy* **2022**, *257*, 124738.
(76) Zhang, Z.; Kusalik, P. G.; Liu, C.; Wu, N. Methane hydrate formation in slit-shaped pores: Impacts of surface hydrophilicity. *Energy* **2023**, *285*, 129414.
(77) Fernández-Fernández, Á. M.; Bárcena, A.; Conde, M. M.; Pérez-Sánchez, G.; Pérez-Rodríguez, M.; Piñeiro, M. M. Modeling oceanic sedimentary methane hydrate growth through molecular dynamics simulation. *J. Chem. Phys.* **2024**, *160*, 144107.
(78) Algaba, J.; Blazquez, S.; Feria, E.; Míguez, J. M.; Conde, M. M.; Blas, F. J. Three-phase equilibria of hydrates from computer simulation. II: Finite-size effects in the carbon dioxide hydrate. *J. Chem. Phys.* **2024**, *160*, 164722.
(79) Algaba, J.; Blazquez, S.; Míguez, J. M.; Conde, M. M.; Blas, F. J. Three-phase equilibria of hydrates from computer simulation. III: Effect of dispersive interactions in methane and carbon dioxide hydrates. *J. Chem. Phys.* **2024**, *160*, 164723.
(80) Blazquez, S.; Algaba, J.; Míguez, J. M.; Vega, C.; Blas, F. J.; Conde, M. M. Three-phase equilibria of hydrates from computer simulation. I: Finite-size effects in the methane hydrate. *J. Chem. Phys.* **2024**, *160*, 164721.
(81) Rowlinson, J. S.; Widom, B. *Molecular Theory of Capillarity*; Claredon Press, 1982.
(82) De Miguel, E.; Jackson, G. Detailed examination of the calculation of the pressure in simulations of systems with discontinuous interactions from the mechanical and thermodynamic perspectives. *Mol. Phys.* **2006**, *104*, 3717−3734.
(83) de Miguel, E.; Jackson, G. The Nature of the Calculation of the Pressure in Molecular Simulations of Continuous Models from Volume Perturbations. *J. Chem. Phys.* **2006**, *125*, 164109.
(84) Flyvbjerg, H.; Petersen, H. Error estimates on averages of correlated data. *J. Chem. Phys.* **1989**, *91*, 461−466.
(85) Buch, V.; Sandler, P.; Sadlej, J. Simulations of H_2O Solid, Liquid, and Clusters, with an Emphasis on Ferroelectric Ordering Transition in Hexagonal Ice. *J. Phys. Chem. B* **1998**, *102*, 8641−8653.
(86) Abascal, J. L. F.; Vega, C. A General Purpose Model for the Condensed Phases of Water: TIP4P/2005. *J. Chem. Phys.* **2005**, *123*, 234505.
(87) Sesé, L. M. Feynman-Hibbs quantum effective potentials for Monte Carlo simulations of liquid neon. *Mol. Phys.* **1993**, *78*, 1167−1177.
(88) Debenedetti, P. G. *Metastable Liquids: Concepts and Principles*; Princeton University Press, 1996.
(89) Walsh, M. R.; Beckham, G. T.; Koh, C. A.; Sloan, E. D.; Wu, D. T.; Sum, A. K. Methane Hydrate Nucleation Rates from Molecular Dynamics Simulations: Effects of Aqueous Methane Concentration, Interfacial Curvature, and System Size. *J. Phys. Chem. C* **2011**, *115*, 21241−21248.
(90) Liang, S.; Kusalik, P. G. Exploring nucleation of H_2S hydrates. *Chem. Sci.* **2011**, *2*, 1286−1292.
(91) Yagasaki, T.; Matsumoto, M.; Andoh, Y.; Okazaki, S.; Tanaka, H. Effect of Bubble Formation on the Dissociation of Methane Hydrate in Water: A Molecular Dynamics Study. *J. Phys. Chem. B* **2014**, *118*, 1900−1906.
(92) Bagherzadeh, S. A.; Alavi, S.; Ripmeester, J.; Englezos, P. Formation of methane nano-bubbles during hydrate decomposition and their effect on hydrate growth. *J. Chem. Phys.* **2015**, *142*, 214701.
(93) Fang, B.; Moultos, O.; Lü, T.; Sun, J.; Liu, Z.; Ning, F.; Vlugt, T. J. H. Effects of nanobubbles on methane hydrate dissociation: A molecular simulation study. *Fuel* **2023**, *345*, 128230.
(94) Kashchiev, D.; Firoozabadi, A. Driving force for crystallization of gas hydrates. *J. Cryst. Growth* **2002**, *241*, 220−230.
(95) Kashchiev, D.; Firoozabadi, A. Nucleation of gas hydrates. *J. Cryst. Growth* **2002**, *243*, 476−489.
(96) Kashchiev, D.; van Rosmalen, G. M. Review: Nucleation in solutions revisited. *Cryst. Res. Technol.* **2003**, *38*, 555−574.

https://doi.org/10.1021/acs.energyfuels.5c01012
Energy Fuels 2025, 39, 15184−15197